Journal of Theoretical Biology 267 (2010) 106–120

Contents lists available at ScienceDirect

Journal of Theoretical Biology

journal homepage: www.elsevier.com/locate/yjtbi

# Non-local models for the formation of hepatocyte–stellate cell aggregates

J.E.F. Green [a,b,*], S.L. Waters [c,b], J.P. Whiteley [d], L. Edelstein-Keshet [e], K.M. Shakesheff [f], H.M. Byrne [b]

[a] Computational Biology Group, School of Computer Science and Software Engineering, Faculty of Engineering, Computing and Mathematics, The University of Western Australia, 35 Stirling Highway, Crawley, WA 6009, Australia
[b] Centre for Mathematical Medicine and Biology, School of Mathematical Sciences, University of Nottingham, Nottingham NG7 2RD, UK
[c] Oxford Centre for Industrial and Applied Mathematics, Mathematical Institute, University of Oxford, 24-29 St Giles', Oxford OX1 3LB, UK
[d] Oxford University Computing Laboratory, Wolfson Building, Parks Road, Oxford OX1 3QD, UK
[e] Department of Mathematics, University of British Columbia, Vancouver, British Columbia, Canada V6T 1Z2
[f] Tissue Engineering Group, School of Pharmacy, University of Nottingham, Nottingham NG7 2RD, UK

ARTICLE INFO

*Article history:*
Received 19 February 2010
Received in revised form
10 August 2010
Accepted 10 August 2010
Available online 13 August 2010

*Keywords:*
Cell aggregation
Chemotaxis
Tissue engineering
Integro-differential equations

ABSTRACT

Liver cell aggregates may be grown *in vitro* by co-culturing hepatocytes with stellate cells. This method results in more rapid aggregation than hepatocyte-only culture, and appears to enhance cell viability and the expression of markers of liver-specific functions. We consider the early stages of aggregate formation, and develop a new mathematical model to investigate two alternative hypotheses (based on evidence in the experimental literature) for the role of stellate cells in promoting aggregate formation. Under Hypothesis 1, each population produces a chemical signal which affects the other, and enhanced aggregation is due to chemotaxis. Hypothesis 2 asserts that the interaction between the two cell types is by direct physical contact: the stellates extend long cellular processes which pull the hepatocytes into the aggregates. Under both hypotheses, hepatocytes are attracted to a chemical they themselves produce, and the cells can experience repulsive forces due to overcrowding. We formulate non-local (integro-partial differential) equations to describe the densities of cells, which are coupled to reaction–diffusion equations for the chemical concentrations. The behaviour of the model under each hypothesis is studied using a combination of linear stability analysis and numerical simulations. Our results show how the initial rate of aggregation depends upon the cell seeding ratio, and how the distribution of cells within aggregates depends on the relative strengths of attraction and repulsion between the cell types. Guided by our results, we suggest experiments which could be performed to distinguish between the two hypotheses.

© 2010 Elsevier Ltd. All rights reserved.

## 1. Introduction

At present there are few treatments for chronic liver disease, organ transplant being the most successful. However, a lack of suitable donor organs means that interest is turning to the development of liver support devices. As a result, increasing research effort is being focused on the *in vitro* engineering of liver tissue for such devices, as well as for drug testing and, potentially, for transplantation (Green et al., 2009). Approximately 80% of a healthy liver is composed of hepatocytes (Mitaka, 1998), cells which perform most of its biological functions (Selden et al., 1999). The liver contains at least four other cell types including stellate cells (also known as Ito cells), which are thought to play an important role in hepatic regeneration *in vivo*; hence there is interest in their potential use in liver tissue engineering *in vitro* (Bhandari et al., 1997; Riccalton-Banks et al., 2003; Thomas et al., 2005). A number of studies suggest that cell–cell contact between hepatocytes, and between hepatocytes and other cell types, is key to maintaining the viability and functionality of liver tissue grown *in vitro*. Such contacts are promoted by culture techniques that result in the formation of spheroidal cell aggregates (Abu-Absi et al., 2002; Riccalton-Banks, 2002; Richert et al., 2002; Thomas et al., 2005). Our aim in this paper is to use mathematical modelling to investigate the effect of hepatocyte–stellate cell interactions on the aggregation process.

When hepatocytes and stellate cells are co-cultured, cell aggregates form more rapidly and retain liver-specific functions (such as albumin production and cytochrome P450 activity) for a longer period than when the hepatocytes are cultured alone (Krause et al., 2009; Riccalton-Banks et al., 2003; Riccalton-Banks, 2002; Thomas et al., 2005). One mechanism that may contribute to enhanced aggregation is chemotaxis. Hepatocytes are known to respond chemotactically to hepatocyte growth factor (HGF) *in vitro* (Stolz and Michalopoulos, 1997), and stellate cells from rats produce HGF when stimulated with hepatocyte-conditioned medium (Skrtic et al., 1999). In fact, stimulation with just one

* Corresponding author at: Computational Biology Group, School of Computer Science and Software Engineering, Faculty of Engineering, Computing and Mathematics, The University of Western Australia, 35 Stirling Highway, Crawley, WA 6009, Australia.
*E-mail address:* edward.green@uwa.edu.au (J.E.F. Green).

0022-5193/$ - see front matter © 2010 Elsevier Ltd. All rights reserved.
doi:10.1016/j.jtbi.2010.08.013

component of the hepatocyte-conditioned medium, insulin-like growth factor-1 (IGF-1), was sufficient to cause the stellate cells to produce HGF. Another study, by Gentilini et al. (2000), reported that IGF-1 is a chemoattractant for human hepatic stellate cells. Hence there may be a feedback loop between the two cell types: the hepatocytes produce insulin-like growth factor-1 which attracts the stellates, and stimulates them to produce more HGF. HGF then acts as a chemoattractant for the hepatocytes, leading to the formation of heterogeneous cell aggregates.

An alternative explanation has been put forward by Thomas et al. (2006). Time-lapse video footage reveals that stellates extend long processes, which, on contact with an hepatocyte, appear to pull the cell into the nascent aggregate (Fig. 1). We speculate that this physical contact between the two cells types promotes aggregation. It is possible that the action of the processes is provoked by a chemical factor secreted by the hepatocytes, as mono-cultured stellates stimulated with hepatocyte-conditioned medium retracted their processes (as they do when pulling heptocytes into an aggregate), whilst this did not occur when the conditioned medium was absent. Furthermore, aggregates formed more slowly, and were less well defined, when the stellates were co-cultured with cells of the Hep G2 cell line (hepatocellular carcinoma cells) rather than hepatocytes, suggesting an interaction specific to these particular cell types. However, the stellates exhibited the same contractile response to hepatocyte fragments as to whole cells, which suggests that the retraction of the processes is not solely due to the secretion of chemical factors by hepatocytes. Thomas et al. (2006) suggest that the attraction between stellate cells is negligible. Stellate cells in monoculture were found to have low cell motility compared to those in co-culture, and did not form aggregates (*e.g.* see Thomas et al., 2006, Fig. 4).

In this paper, we use mathematical modelling to explore the two hypotheses outlined above for hepatocyte–stellate cell interactions. Our model accounts for chemical signalling between the two cell types, the forces exerted by the stellates' cellular processes, and the effects of overcrowding, which causes cells to repel each other when they become too densely packed. We adopt an approach which combines a Keller–Segel modelling framework to describe chemotactic movement with non-local (integro-differential) terms to represent cell–cell interactions due to overcrowding or the action of the stellates' processes on hepatocytes. Similar non-local terms have previously been used to model differential adhesion in cell sorting experiments (Armstrong et al.,

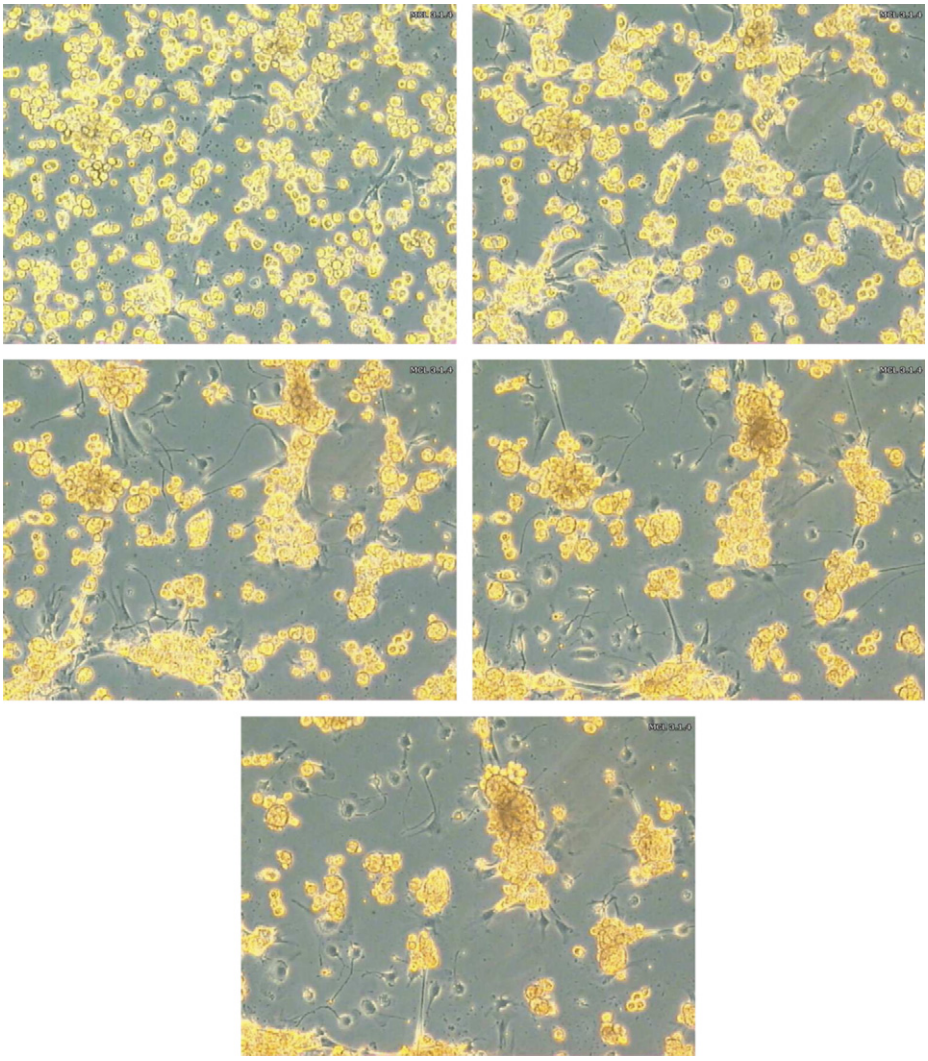

**Fig. 1.** Snapshots from time-lapse video of an hepatocyte–stellate cell co-culture during aggregation. The hepatocytes appear yellow, and have a rounded morphology. Stellates appear grey, but their long cellular processes are clearly distinguishable. The images show an area approx 1000 μm × 700 μm and were taken at approximately 5-hourly intervals (total time elapsed: approx. 21 h). (Images courtesy of Robert Thomas, Tissue Engineering Group. Similar images, including later timepoints, are shown in Thomas et al. (2006). Timelapse video footage is also available at: www.ecmjournal.org/journal/papers/vol011/vol011a03.php). (For interpretation of the references to color in this figure legend, the reader is referred to the web version of this article.)

2006; Sherratt et al., 2008), cancer invasion (Gerisch and Chaplain, 2008; Szymanska et al., 2009), and to describe interactions within a social aggregate (such as a swarm) consisting of a homogeneous population (Mogilner and Edelstein-Keshet, 1999). Other applications have included *Myxobacteria* aggregation (Mogilner, 1995), and ecological problems (Billingham, 2004; Gourley et al., 2001). To illustrate the form of these non-local terms, we consider a simple example in which a single population of density $C$ moves in a one dimensional Cartesian geometry by a combination of random motion and advection so that

$$\frac{\partial C}{\partial t}+\frac{\partial}{\partial x}(vC)=D\frac{\partial^2 C}{\partial x^2}, \tag{1.1a}$$

where $D$ is the random motility coefficient, and $v$ is the density-dependent velocity of the cells, which is related to $C$ via a convolution integral:

$$v(x,t)=K*C\equiv\int_\Omega K(x-y)C(y,t)\,dy. \tag{1.1b}$$

The velocity at a position $x$ thus depends upon the density of individuals in a neighbourhood $\Omega$ surrounding $x$. In (1.1b), the kernel function $K$ weights the effect of interactions according to distance (usually, interactions between nearby individuals have greater effect). $K(x-y)$ is generally assumed to be proportional to the force exerted on an individual at $x$ by another at $y$ (Mogilner, 1995). (However, a formal momentum balance is not usually stated in this type of model.) The kernels are prescribed functions of the spatial variable, and, in the absence of environmental biases, are assumed to be odd functions of their argument because we expect individuals to the right of $x$ to induce a velocity of the opposite sign to that induced by individuals to the left of $x$ (see Fig. 2).

The choice of kernel function is key to determining the behaviour of the system; whilst an odd kernel describes aggregation in a swarm (or aggregate) whose centre of mass is stationary, an even kernel gives rise to collective movement (Mogilner and Edelstein-Keshet, 1999). When the kernel includes an even component, travelling wave solutions of the model can be found, provided the odd part of the kernel is sufficiently small (Mogilner, 1995; Mogilner and Edelstein-Keshet, 1999). In Mogilner (1995), analysis of the bifurcation structure of the model for a particular choice of odd kernel reveals that both large scale aggregations (having wavenumbers close to zero) and periodic patterns may arise, depending on the strengths and ranges of attraction and repulsion. In the latter case, the onset of patterning close to bifurcation is studied using a weakly nonlinear analysis.

An alternative model for inter-individual interactions in a social aggregate is presented in Mogilner et al. (2003). There, a Lagrangian (individual-based) approach is adopted, with each member of the swarm treated as a point mass whose movements are governed by the pairwise sum of its interactions with the other swarm members. The model is written as

$$\frac{d\boldsymbol{x}_i}{dt}=\sum_{i\neq j}\boldsymbol{F}(\boldsymbol{x}_i-\boldsymbol{x}_j), \tag{1.2}$$

where $\boldsymbol{x}_i$ is the position of the $i$th member of the swarm, $\boldsymbol{F}$ is the interaction force on the $i$th individual due to a neighbour at $x_j$, and

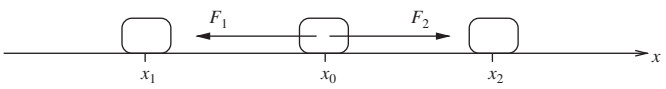


**Fig. 2.** Forces $F_1$ and $F_2$ acting on a cell at $x_0$ due to attraction to cells at $x_1$ and $x_2$, respectively. When the cells are evenly spaced ($x_0-x_1=x_2-x_0$), the magnitudes of the forces are equal ($F_1=F_2$).

$i,\ j=1,2,\ldots,N$ ($N$ being the number of members of the swarm). Hence (1.2) can be viewed as a force balance between inter-individual forces and drag, where inertial effects are assumed negligible, and the units are so chosen that the constant of proportionality (*i.e.* drag coefficient) is unity.

Bodnar and Velazquez (2005) have formally established that, in the one-dimensional case, models of the form (1.1a) can be derived as macroscopic limits of Lagrangian models such as (1.2), provided the interaction force $\boldsymbol{F}$ is of gradient type (*i.e.* $\boldsymbol{F}=-\nabla W$). In summary, if the lengthscale over which interactions take place (*i.e.* the lengthscale over which $W$ undergoes $O(1)$ variations) is much greater than the typical distance between individuals, then, as $N\to\infty$, one can introduce a density $C$ and replace the sum in Eq. (1.2) by a convolution integral. The macroscopic equation is

$$\frac{\partial C(x,t)}{\partial t}=\frac{\partial}{\partial x}\left(C(x,t)\int_\Omega W'(x-y)C(y,t)\,dy\right), \tag{1.3}$$

which is equivalent to Eq. (1.1a) when $W'=-K$ and $D=0$. Furthermore, if the potential $W$ is repulsive, then the addition of a 'white noise' term to the right-hand side (RHS) of Eq. (1.2) gives rise, in the continuum limit, to a diffusion term on the RHS of Eq. (1.3) (making it equivalent to (1.1a))—although the diffusion coefficient may depend on $C$ for certain choices of $W$ (Bodnar and Velazquez, 2005). The significance of the connection between the individual-based and continuum models is clear: given a knowledge of the interactions between a pair of cells, we can infer the correct form for the interaction kernel in the continuum model (subject to the assumptions about cell spacing and pairwise interactions stated above).

In this paper, we investigate the two hypotheses about hepatocyte–stellate interactions by developing continuum models. We focus on cell–cell interactions, neglecting the effects of the ECM and culture medium (which are considered in Green et al., 2009; Green, 2006). We present a general model (Section 2) which can be specialised to the two hypotheses described above. The behaviour of the model is investigated using a combination of linear stability analysis (Section 3) and numerical simulations (Section 4). For each hypothesis, we determine how the distribution of cells within aggregates depends upon the strengths of attraction and repulsion between the cells. Experimental observations of the cell distribution can thus be used to make inferences about the relative strengths of hepatocyte–hepatocyte, hepatocyte–stellate and stellate-stellate interactions (*c.f.* cell sorting due to differential adhesion (Steinberg, 1963). We also use the model to predict the seeding ratio of hepatocytes to stellate cells that gives the most rapid aggregate formation. The paper concludes in Section 5 with a comparison of our model predictions and recent experimental results, and suggestions for further work.

## 2. Model formulation

We develop a general mathematical model for the aggregation of hepatocytes and stellate cells, which embodies the hypotheses introduced in Section 1. We consider a one-dimensional geometry, $-L<x<L$, and denote the densities of the hepatocytes and stellate cells by $n(x,t)$ and $m(x,t)$, respectively (where $t$ denotes time). For simplicity, proliferation and death of both cell types are neglected. (This appears reasonable for the early stages of cell culture (approximately the first 24 h) in which we are interested; Thomas et al., 2006 found that around 10% of the cells died between 24 and 48 h in culture.) We assume that hepatocytes secrete a chemoattractant (possibly IGF-1), with concentration $c_1(x,t)$, which stimulates their aggregation in the absence of the stellates. We assume that stellates are also attracted to this chemical. In addition, stellates produce a second chemical

(possibly HGF), with concentration $c_2(x,t)$, which acts as a chemoattractant for hepatocytes only. We use the familiar Keller–Segel framework to describe the cells' motion up chemical gradients. We assume, as in Mogilner (1995), that the timescale for diffusion of both chemicals is short compared to that for cell movement, and, hence, that the quasi-steady approximation for $c_1$ and $c_2$ is valid. We also allow for non-local cell–cell interactions, using the integro-PDE framework. These effects include repulsion due to overcrowding and attraction due to the extension of processes by the stellates. Combining these effects, the general model takes the form:

$$\frac{\partial n}{\partial t}+\chi_1^*\frac{\partial}{\partial x}\left(n\frac{\partial c_1}{\partial x}\right)+\chi_2^*\frac{\partial}{\partial x}\left(n\frac{\partial c_2}{\partial x}\right)+\frac{\partial}{\partial x}[n(K_n^**n)+n(K_{nm}^**m)]=D_n^*\frac{\partial^2 n}{\partial x^2}, \tag{2.1a}$$

$$\frac{\partial m}{\partial t}+\phi^*\frac{\partial}{\partial x}\left(m\frac{\partial c_1}{\partial x}\right)+\frac{\partial}{\partial x}[m(K_m^**m)+m(K_{mn}^**n)]=D_m^*\frac{\partial^2 m}{\partial x^2}, \tag{2.1b}$$

$$D_1^*\frac{\partial^2 c_1}{\partial x^2}+\alpha_1^*n-\gamma_1^*c_1=0, \tag{2.1c}$$

$$D_2^*\frac{\partial^2 c_2}{\partial x^2}+\alpha_2^*m-\gamma_2^*c_2=0. \tag{2.1d}$$

The kernel functions describe the non-local interactions between the different populations: $K_{nm}^*$ represents the effect of stellates ($m$) on hepatocytes ($n$); conversely, $K_{mn}^*$ represents the effect of hepatocytes on stellates; $K_n^*$ and $K_m^*$ represent the interactions between members of the same population. $D_n^*$ and $D_m^*$ are the random motility coefficients for the two cell types. The constants $\chi_1^*$ and $\chi_2^*$ represent the sensitivity of the hepatocytes to gradients of $c_1$ and $c_2$, and $\phi^*$ similarly gives the sensitivity of the stellates to gradients of $c_1$. We denote the diffusion coefficients of the two chemicals by $D_1^*$ and $D_2^*$, respectively. We assume they are produced at rates $\alpha_1^*$ and $\alpha_2^*$, and decay at rates $\gamma_1^*$ and $\gamma_2^*$. If we identify $c_2$ with HGF then we should make $\alpha_2^*$ depend on $c_1$ as the results of Skrtic et al. (1999) suggest that the amount of HGF produced increases with increasing IGF-1 concentration. However, for simplicity, we assume here that $\alpha_2^*$ is constant.

### 2.1. Boundary and initial conditions

Eqs. (2.1) are solved subject to the following boundary and initial conditions. We assume that the cell densities are symmetric about $x=0$, and are spatially periodic functions, with period $2L$. The latter condition ensures the convolution terms vanish at the edges of the domain, and thus that the no flux conditions for the cells and chemoattractants at $x=\pm L$ take their familiar forms. The initial and boundary conditions thus read

$$n(x,0)=n_i(x),\quad m(x,0)=m_i(x), \tag{2.2a}$$

$$\left.\frac{\partial n}{\partial x}\right|_{x=\pm L}=\left.\frac{\partial m}{\partial x}\right|_{x=\pm L}=\left.\frac{\partial c_1}{\partial x}\right|_{x=\pm L}=\left.\frac{\partial c_2}{\partial x}\right|_{x=\pm L}=0. \tag{2.2b}$$

### 2.2. Hypothesis 1: hepatocyte–stellate interactions through chemotaxis

We now specialise the above model to the case where the attraction between hepatocytes and stellate cells is caused by diffusible chemicals. Thus all the chemical signalling processes described above are active, and, hence, the chemotaxis coefficients $\chi_1^*$, $\chi_2^*$ and $\phi^*$ are non-zero. The only non-local interactions assumed to take place are due to overcrowding: when cells come close to each other they experience a repulsive force. We thus set

$$K_n^*=K_m^*=K_{nm}^*=K_{mn}^*=K_R^*, \tag{2.3a}$$

where the repulsion kernel, $K_R^*$, takes the form

$$K_R^*(x)=\begin{cases}R^*\left(\dfrac{r^*}{x}-1\right) & \text{if } 0<x\le r^*,\\ R^*\left(\dfrac{r^*}{x}+1\right) & \text{if } -r^*\le x<0,\\ 0 & \text{otherwise.}\end{cases} \tag{2.3b}$$

Thus, the repulsive force has strength $R^*$, and is experienced only when cells come within a range $r^*$ of each other (measured as the distance between their centres). As the distance between the cells tends to zero, the repulsive force becomes arbitrarily large (see Fig. 3(a)). For simplicity, we have assumed that the strength of repulsive interactions is independent of the type of cells involved. Differences in cell size or the strength of cell–substrate adhesion between the two cell types mean that this assumption may not hold in practice. However, it could easily be relaxed by taking different values of $R^*$ and $r^*$ for each of the four kernels. We postpone such considerations for future work.

### 2.3. Hypothesis 2: hepatocyte–stellate interactions via direct physical contact

Here, we assume that hepatocyte–stellate attraction is due to direct physical contact. Hepatocytes again aggregate via

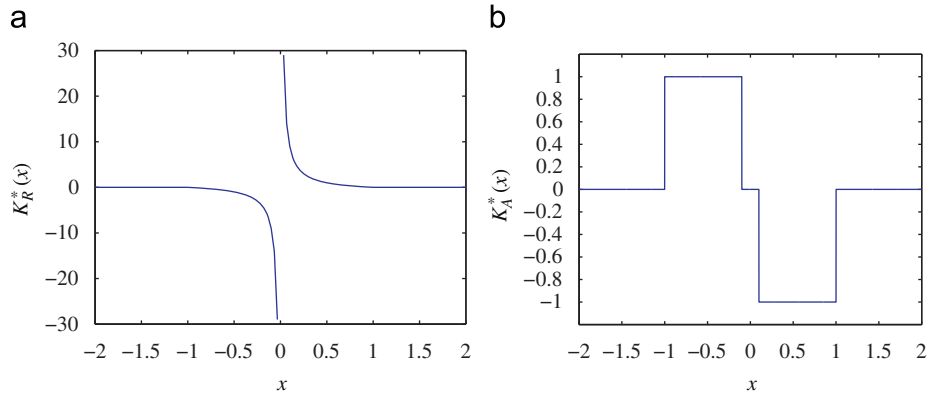


**Fig. 3.** Sketches of the kernel functions used to describe repulsive and attractive cell–cell interactions, respectively. (a) Repulsion kernel $K_R^*(x)$ with $R^*=r^*=1$—see Eq. (2.3b). (b) Hepatocyte–stellate attraction kernel $K_A^*(x)$ with $A_2^*=a_2^*=1$, $r^*=0.1$—see Eq. (2.4d).

chemotaxis in response to a diffusible signalling molecule that they produce, but chemical signalling between hepatocytes and stellates is neglected. Thus, in Eqs. (2.1) we fix

$$\chi_1^* > 0, \quad \chi_2^* = 0, \quad \phi^* = 0. \tag{2.4a}$$

As before (see Eq. (2.3)), all cells, regardless of type, repel each other if they are too close. However, we assume additionally that stellate cells exert attractive forces on hepatocytes if the latter come within range of their processes. The hepatocyte–stellate and stellate-hepatocyte interaction forces are thus of the same form. For simplicity, we shall assume they are also of the same magnitude, and hence write $K_{mn}=K_{nm}$. (This assumption neglects the possibility that one of the cell types may be larger or more strongly adherent to the ECM than the other. However, it is consistent with our earlier assumption about the strength of the repulsive force.) We suppose that the stellates exert a constant attractive force on the hepatocytes when they are within a finite range of each other. Combining the above effects, we employ the following forms for the kernels

$$K_n^* = K_m^* = K_R^*, \tag{2.4b}$$

$$K_{nm}^* = K_{mn}^* = K_R^* + K_A^*, \tag{2.4c}$$

where

$$K_A^*(x) = \begin{cases} -A_2^* & \text{if } r^* \le x \le a_2^*, \\ A_2^* & \text{if } -a_2^* \le x \le -r^*, \\ 0 & \text{otherwise,} \end{cases} \tag{2.4d}$$

and $K_R^*$ is defined in Eq. (2.3b). In (2.4d), the constant $A_2^*$ represents the strength of stellate-hepatocyte attraction, $a_2^*$ is the average length of a stellate cellular process (and represents the typical range of attraction) and $r^*$ is the range of repulsion, as defined earlier. The function $K_A^*$ is plotted in Fig. 3.

We note that under Hypothesis 2, Eq. (2.1d) for $c_2$ decouples, since when $\chi_2^*=0$, $c_2$ has no effect on cell behaviour. Hence, under this hypothesis we need only solve Eqs. (2.1a)–(2.1c).

### 2.4. Non-dimensionalisation

We non-dimensionalise Eqs. (2.1) as follows (with tildes indicating dimensionless quantities):

$$x = \lambda\tilde{x}, \quad t = T\tilde{t}, \quad n = n_s\tilde{n}, \quad m = n_s\tilde{m}, \quad c_1 = \frac{\alpha_1^* n_s}{\gamma_1^*}\tilde{c_1}, \quad c_2 = \frac{D_1^*\alpha_2^* n_s}{D_2^*\gamma_1^*}\tilde{c_2},$$

$$(K_n^*, K_m^*, K_{nm}^*, K_{mn}^*) = \frac{\chi_1^*\alpha_1^*}{D_1^*}(\tilde{K}_n, \tilde{K}_m, \tilde{K}_{nm}, \tilde{K}_{mn}),$$

where

$$\lambda = \sqrt{\frac{D_1^*}{\gamma_1^*}}, \quad T = \frac{D_1^*}{\chi_1^*\alpha_1^* n_s},$$

and $n_s$ is a typical initial cell seeding density. In the above we have thus taken as our lengthscale ($\lambda$) the diffusion lengthscale of $c_1$, and our timescale ($T$) is the timescale of hepatocyte aggregation by chemotaxis in response to other hepatocytes. The dimensionless system is then (dropping tildes)

$$\frac{\partial n}{\partial t} + \frac{\partial}{\partial x}\left(n\frac{\partial c_1}{\partial x}\right) + \chi_2\frac{\partial}{\partial x}\left(n\frac{\partial c_2}{\partial x}\right) + \frac{\partial}{\partial x}[n(K_n * n) + n(K_{nm} * m)] = D_n\frac{\partial^2 n}{\partial x^2}, \tag{2.5a}$$

$$\frac{\partial m}{\partial t} + \phi\frac{\partial}{\partial x}\left(m\frac{\partial c_1}{\partial x}\right) + \frac{\partial}{\partial x}[m(K_m * m) + m(K_{mn} * n)] = D_m\frac{\partial^2 m}{\partial x^2}, \tag{2.5b}$$

$$\frac{\partial^2 c_1}{\partial x^2} + n - c_1 = 0, \tag{2.5c}$$

$$\frac{\partial^2 c_2}{\partial x^2} + m - \gamma_2 c_2 = 0, \tag{2.5d}$$

where we have introduced the following dimensionless parameters

$$\chi_2 = \frac{\chi_2^* D_1^*}{\chi_1^* D_2^*}, \quad \phi = \frac{\phi^*}{\chi_1^*}, \quad D_n = \frac{D_n^*\gamma_1^*}{\chi_1^*\alpha_1^* n_s}, D_m = \frac{D_m^*\gamma_1^*}{\chi_1^*\alpha_1^* n_s},$$
$$\gamma_2 = \frac{\gamma_2^* D_1^*}{\gamma_1^* D_2^*}, \quad \varepsilon = \frac{\sqrt{D_1^*}}{L\sqrt{\gamma_1^*}}, \tag{2.6}$$

so that $\chi_2$ and $\phi$ are the dimensionless chemotaxis coefficients, $D_n$ and $D_m$ are ratios of the timescales of aggregation and random movement for the two cell types, $\gamma_2$ is the dimensionless decay rate of $c_2$ and $\varepsilon$ is the ratio of the aggregate lengthscale to the domain length. Under this rescaling, the domain in which the dimensionless equations (2.5) are solved is thus $-1/\varepsilon < x < 1/\varepsilon$.

The dimensionless kernels are

$$K_R(x) = \begin{cases} R\left(\frac{r}{x} - 1\right) & \text{if } 0 < x \le r, \\ R\left(\frac{r}{x} + 1\right) & \text{if } -r \le x < 0, \\ 0 & \text{otherwise,} \end{cases} \tag{2.7a}$$

$$K_A = \begin{cases} -A_2 & \text{if } r \le x \le a_2, \\ A_2 & \text{if } -a_2 \le x \le -r, \\ 0 & \text{otherwise,} \end{cases} \tag{2.7b}$$

where we have introduced the dimensionless parameters

$$r = \sqrt{\frac{\gamma_1^*}{D_1^*}}r^*, \quad R = \frac{R^* D_1^*}{\chi_1^*\alpha_1^*}, \quad A_2 = \frac{A_2^* D_1^*}{\chi_1^*\alpha_1^*}, \quad a_2 = \sqrt{\frac{\gamma_1^*}{D_1^*}}a_2^*. \tag{2.8}$$

In (2.8), $R$ and $r$ are the dimensionless strength and range of repulsion, respectively; $A_2$ represents the strength of the attraction between hepatocytes and stellates, whilst $a_2$ is the average dimensionless length of a stellate cellular process (hence representing the typical range of attraction).

In the absence of suitable experimental data, it is impossible to give precise values for many of the parameters introduced above. Since the random motility coefficients for hepatocytes and stellates have not been measured, we use published data for other cell types to estimate the orders of magnitude of $D_n$ and $D_m$. Luca et al. (2003) report that microglia (a type of cell found in the brain) have a diffusivity of $33\,\mu m^2\,min^{-1}$ ($=5.5\times10^{-9}\,cm^2\,s^{-1}$), whilst for microvessel endothelial cells, Stokes et al. (1990) report values in the approximate range $5–8\times10^{-9}\,cm^2\,s^{-1}$, depending upon the concentration of a chemical in the culture medium. We note that the cell aggregation timescale, $T$, is of the order of several hours to one day ($\approx10^4-10^5$ s), and the lengthscale of an aggregate, $\lambda$, is around $100\,\mu m = 10^{-2}$ cm (Green et al., 2009). Combining these values gives estimates for the dimensionless parameters $D_n$ and $D_m$ of 0.1–1.0. The quantities $\chi_2$ and $\phi$ represent relative chemotactic affinities for hepatocyte–stellate interactions, compared to hepatocyte–hepatocyte interactions. As a first approximation, we suppose that these effects are equally important, and take $\chi_2, \phi = O(1)$. The relative diffusive lengthscale of the chemical $c_2$ is taken to be similar to that for $c_1$, *i.e.* $\gamma_2 = O(1)$. For similar reasons, we take the strength of the hepatocyte–stellate attraction due to cell–cell interaction, $A_2$, and its range, $a_2$, to be $O(1)$. However, as repulsion is considered to be due to overcrowding, we assume it is strong and short-ranged (as in Mogilner et al., 2003), and hence we take $r \ll 1 \ll R$. Finally, as in Green et al. (2009), we take the length, $L$, of the domain to be of the order of 1 cm, based on the typical radius of a culture well. This gives $\varepsilon = O(10^{-2})$.

**Table 1**
Summary of how the assumptions associated with the two hypotheses influence the system parameters and the functional forms of the kernels (see Eqs. (2.5) and (2.7)).

| Parameter/Kernel | Assumption | |
|---|---|---|
| | Hypothesis 1 | Hypothesis 2 |
| $\chi_2$ | $>0$ | 0 |
| $\phi$ | $>0$ | 0 |
| $K_n$ | $K_R$ | $K_R$ |
| $K_m$ | $K_R$ | $K_R$ |
| $K_{nm}$ | $K_R$ | $K_R + K_A$ |
| $K_{mn}$ | $K_R$ | $K_R + K_A$ |

The boundary conditions now become

$$\left.\frac{\partial n}{\partial x}\right|_{x=\pm 1/\varepsilon} = \left.\frac{\partial m}{\partial x}\right|_{x=\pm 1/\varepsilon} = \left.\frac{\partial c_1}{\partial x}\right|_{x=\pm 1/\varepsilon} = \left.\frac{\partial c_2}{\partial x}\right|_{x=\pm 1/\varepsilon} = 0, \tag{2.9}$$

where the period of $n$ and $m$ is now $2/\varepsilon$.

In the limit as $\varepsilon \to 0$ it is possible to solve for $c_1$ and $c_2$ in terms of $n$ and $m$ using Green's functions (Lee et al., 2001; Luca et al., 2003). For a domain of infinite spatial extent, we have

$$c_1(x,t) = \frac{1}{2}\int_{-\infty}^{\infty} n(y,t)\exp(-|x-y|)\,dy, \tag{2.10a}$$

$$c_2(x,t) = \frac{1}{2\sqrt{\gamma_2}}\int_{-\infty}^{\infty} m(y,t)\exp(-\sqrt{\gamma_2}|x-y|)\,dy. \tag{2.10b}$$

Using (2.10), the chemotaxis terms in Eqs. (2.5) resemble the non-local interaction terms. We exploit this result to simplify our linear stability analysis in Section 3.

For subsequent reference, the main assumptions (in terms of the dimensionless chemotaxis parameters and kernel forms) of the two hypotheses are summarised in Table 1.

## 3. Linear stability analysis

We now investigate the linear stability of spatially uniform steady states of the model equations in order to determine the parameter regimes in which we may expect to see aggregation. We consider an infinite domain ($\varepsilon = \lambda/L \to 0$) so that we can absorb the chemotaxis terms into the non-local terms by employing a suitably modified kernel (Mogilner, 1995). We then need only consider the system

$$\frac{\partial n}{\partial t} + \frac{\partial}{\partial x}[n(K_n * n) + n(K_{nm} * m)] = D_n\frac{\partial^2 n}{\partial x^2}, \tag{3.1a}$$

$$\frac{\partial m}{\partial t} + \frac{\partial}{\partial x}[m(K_m * m) + m(K_{mn} * n)] = D_m\frac{\partial^2 m}{\partial x^2}. \tag{3.1b}$$

We investigate the spatially homogeneous steady state, $n = n_0$, $m = m_0$ which approximates the conditions immediately after the cells are seeded in the culture wells, and introduce small perturbations of the form

$$n = n_0 + \hat{n}(x,t), \quad m = m_0 + \hat{m}(x,t), \tag{3.2}$$

where $|\hat{n}|$, $|\hat{m}| \ll 1$. We substitute these forms into the governing Eqs. (3.1) and linearise to obtain

$$\frac{\partial \hat{n}}{\partial t} = D_n\frac{\partial^2 \hat{n}}{\partial x^2} - n_0\frac{\partial}{\partial x}(K_{nm} * \hat{m} + K_n * \hat{n}), \tag{3.3a}$$

$$\frac{\partial \hat{m}}{\partial t} = D_m\frac{\partial^2 \hat{m}}{\partial x^2} - m_0\frac{\partial}{\partial x}(K_{mn} * \hat{n} + K_m * \hat{m}). \tag{3.3b}$$

In writing (3.3) we have exploited the fact that terms containing convolutions with constant densities, *e.g.* $K_{nm} * m_0$ vanish, since the kernels are assumed to be odd.

We now set

$$\hat{n} = n_1 e^{(iqx+\omega t)}, \quad \hat{m} = m_1 e^{(iqx+\omega t)}, \tag{3.4}$$

where $q$ and $\omega$ are, respectively, the wavenumber and growth rate of the perturbation, and $|n_1|$, $|m_1| \ll 1$. It is straightforward to show that the convolution terms can be written

$$K_n * \hat{n} = n_1\int_{-\infty}^{\infty} K_n(x-y)e^{(iqy+\omega t)}\,dy = n_1 e^{(iqx+\omega t)}\tilde{K}_n(q), \tag{3.5}$$

where $\tilde{K}_n(q)$ denotes the Fourier transform of $K_n$, defined as

$$\tilde{K}_n(q) = \int_{-\infty}^{\infty} K_n(x)e^{-iqx}\,dx.$$

We note that since the kernels are odd functions of their argument, their Fourier transforms are imaginary.

Substituting (3.4) into Eqs. (3.3) we obtain

$$\boldsymbol{J}\begin{pmatrix} n_1 \\ m_1 \end{pmatrix} = \mathbf{0}, \tag{3.6}$$

where

$$\boldsymbol{J} = \begin{pmatrix} \omega + D_n q^2 + iqn_0\tilde{K}_n & iqn_0\tilde{K}_{nm} \\ iqm_0\tilde{K}_{mn} & \omega + D_m q^2 + iqm_0\tilde{K}_m \end{pmatrix}. \tag{3.7}$$

For non-trivial solutions, $(n_1, m_1) \neq \mathbf{0}$, we require $\det(\boldsymbol{J}) = 0$, which leads to a quadratic dispersion relation of the form

$$\omega^2 + B\omega + C = 0, \tag{3.8}$$

where

$$B = q^2(D_n + D_m) + iq(n_0\tilde{K}_n + m_0\tilde{K}_m), \tag{3.9a}$$

$$C = (D_n q^2 + iqn_0\tilde{K}_n)(D_m q^2 + iqm_0\tilde{K}_m) + q^2 n_0 m_0 \tilde{K}_{nm}\tilde{K}_{mn}. \tag{3.9b}$$

We note that, since interactions between cells of the same type are identical under both hypotheses, so are the modified versions of $K_n$ and $K_m$, which are given by

$$K_n(x) = -\left(\frac{1}{2}\right)\mathrm{sign}(x)\exp(-|x|) + K_R(x), \tag{3.10a}$$

$$K_m(x) = K_R(x), \tag{3.10b}$$

where the first term on the RHS of Eq. (3.10a) arises from the incorporation of hepatocyte–hepatocyte chemotaxis into the kernel. The Fourier transforms are

$$\tilde{K}_n(q) = \frac{iq}{q^2+1} - 2iRr\Psi(qr), \tag{3.11a}$$

$$\tilde{K}_m(q) = -2iRr\Psi(qr). \tag{3.11b}$$

In (3.11), the function $\Psi(\cdot)$, which is plotted in Fig. 4, denotes the Fourier transform of the repulsion kernel (2.7a), so that

$$\Psi(x) = Si(x) - \frac{1}{x}(1-\cos x), \tag{3.12}$$

where $Si(x)$ is the sine integral (Abramowitz and Stegun, 1970)

$$Si(x) = \int_0^x \frac{\sin t}{t}\,dt.$$

With $\tilde{K}_n$ and $\tilde{K}_m$ defined by (3.11), Eq. (3.9a) gives

$$B = q^2\left(D_n + D_m - \frac{n_0}{q^2+1}\right) + 2q(n_0+m_0)Rr\Psi(qr). \tag{3.13}$$

We note that the function $C$ defined by (3.9b) takes different forms under the two hypotheses, and is hence presented in

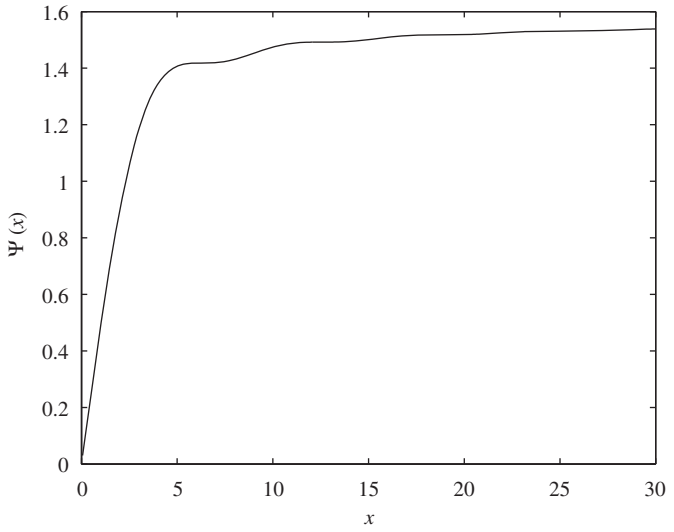


**Fig. 4.** A plot of the function $\Psi(x)$ (see Eq. (3.12)).

Sections 3.1 and 3.2, where the behaviour under each hypothesis is considered in turn.

In order to identify the regions of parameter space in which instability can occur, we first determine the most unstable wavenumber of the system (*i.e.* the value $q_c$ of $q$ which maximises $\Re(\omega)$) and define $\omega_{\max} \equiv \Re(\omega(q_c))$. We then partition the parameter space into regions where the spatially uniform steady state is linearly stable to perturbations of all wavenumbers ($\omega_{\max} < 0$) and others where it is linearly unstable to perturbations of certain wavenumbers ($\omega_{\max} > 0$). In simple cases this can be done analytically. (We note that it may be possible to derive sufficient conditions for the uniform state to be linearly stable in more general cases. However, because a spatially uniform steady state is biologically undesirable, we do not attempt it here.) In general, however, we use the following procedure to determine the regions numerically. We first choose two parameters of interest (*e.g.* $n_0$ and $\chi_2$) and create a rectangular array of pairs of these values (the other system parameters being held fixed). We note that the sum of the roots of equation (3.8) is given by $-B$ and the product by $C$. Thus, for a particular pair of parameter values, if there exists a $q$ such that $C(q) < 0$, then the dispersion relation has one real positive and one real negative root, and the spatially uniform steady state is unstable. We thus evaluate $\min C(q)$ (for a range of values of $q$) for each pair of parameter values in our array; if $\min(C(q)) < 0$ for a particular pair, we colour the relevant square in the array white. The region of the array where $\min C(q) > 0$ is then further subdivided. If $\min(C(q)) > 0$ and $\min(B(q)) < 0$, then for the parameter values in question, there exist wavenumbers for which the spatially uniform steady state is unstable; if $\min(C(q)) > 0$ and $\min(B(q)) > 0$, then the spatially uniform steady state is stable to perturbations of all wavenumbers. In fact, each of the latter two regions may be further subdivided, into regions where all the roots are real ($\min(B^2 - 4C) > 0$) and those where there may be complex conjugate roots ($\min(B^2 - 4C) < 0$).

In the following sections, we consider the stability of the spatially uniform steady state under each hypothesis.

### 3.1. Hypothesis 1

Incorporating the chemotaxis terms into the kernel functions $K_{nm}$ and $K_{mn}$ gives

$$K_{nm}(x) = -\left(\frac{\chi_2}{2}\right)\mathrm{sign}(x)\exp\left(-\left(\frac{|x|}{a}\right)\right) + K_R(x), \tag{3.14a}$$

$$K_{mn}(x) = -\left(\frac{\phi}{2}\right)\mathrm{sign}(x)\exp(-|x|) + K_R(x), \tag{3.14b}$$

where $a = 1/\sqrt{\gamma_2}$ is the dimensionless attraction range of $c_2$. It is straightforward to show that the associated Fourier transforms are

$$\tilde{K}_{nm}(x) = \frac{iq\chi_2 a^2}{a^2q^2+1} - 2iRr\Psi(qr), \tag{3.15a}$$

$$\tilde{K}_{mn}(x) = \frac{iq\phi}{q^2+1} - 2iRr\Psi(qr). \tag{3.15b}$$

For simplicity, we first consider the case for which repulsion effects are negligible ($R=0$). The coefficient $C$ in the dispersion relation (3.8) is then

$$C = q^4\left[D_m\left(D_n - \frac{n_0}{q^2+1}\right) - \frac{n_0 m_0 \chi_2 \phi a^2}{(q^2+1)(a^2q^2+1)}\right]. \tag{3.16}$$

A sufficient condition for instability to occur is $C < 0$, or equivalently,

$$D_m\left(D_n - \frac{n_0}{q^2+1}\right) < \frac{n_0 m_0 \chi_2 \phi a^2}{(q^2+1)(a^2q^2+1)}. \tag{3.17}$$

Thus, in order for instability to arise, chemotaxis must dominate random motion of the two cell populations. If $m_0\chi_2\phi = 0$, then condition (3.17) reduces to $D_n < n_0/(q^2+1)$, which is equivalent to the condition for instability in a model for chemotactic aggregation of a single population of cells. We remark that whilst the case $B < 0 < C$ could give rise to instability, in practice it cannot occur for the following reason. If $B < 0$, then

$$\frac{n_0}{q^2+1} > D_n + D_m \geq D_n, \tag{3.18}$$

and the first term of Eq. (3.16) is non-positive, which means that $C \leq 0$. (However, the case $B < 0, C = 0$, corresponding to $\omega$ having one zero and one positive root is possible, but only if $D_m = 0$ and some other parameter *e.g.* $\chi_2$ is also zero.) Thus, for $D_m > 0$, inequality (3.17) is both necessary and sufficient for instability to occur.

In the limit as $q \to \infty$, $C > 0$ so the spatially uniform steady state is linearly stable to perturbations of sufficiently large wavenumber. We note that the zeros of $C$ are $q = 0$ and the roots of the expression

$$q^4 D_n D_m a^2 + q^2 D_m(D_n + D_n a^2 - n_0 a^2) + D_n D_m - n_0 D_m - n_0 m_0 \chi_2 \phi a^2 = 0, \tag{3.19}$$

which, for convenience, we view as a quadratic for $q^2$. For instability to occur, (3.17) must be satisfied, and hence the roots of (3.19) have differing sign. Thus we conclude that instability will occur for a finite range of wavenumbers $0 < q^2 < q^2_{\max}$, where $q^2_{\max}$ is the positive root of (3.19).

Assuming that $D_m > 0$, we note that by, for example, increasing $\chi_2$, we can decrease $C$ from $C > 0$ to $C < 0$. In this case, one of the two negative real roots of Eq. (3.8) becomes positive so we have a saddle-node bifurcation as $C$ passes through $C = 0$. (Note that we have established above that we cannot have $B < 0 < C$, and hence this is the only type of bifurcation that the model can exhibit in this case.)

When repulsion effects are neglected ($R = 0$), it is straightforward to show that $C(q) < 0$ for certain values of $q$ only if the following inequality is satisfied:

$$D_m(D_n - n_0) < n_0 m_0 \chi_2 \phi a^2.$$

With $m_0 = 1 - n_0$ (*i.e.* assuming that the total cell seeding density is unity), we deduce that the curve partitioning the stable and unstable regions of parameter space is given by

$$n_0^2 - n_0\left(1 + \frac{D_m}{\chi_2\phi a^2}\right) + \frac{D_n D_m}{\chi_2 \phi a^2} = 0. \tag{3.20}$$

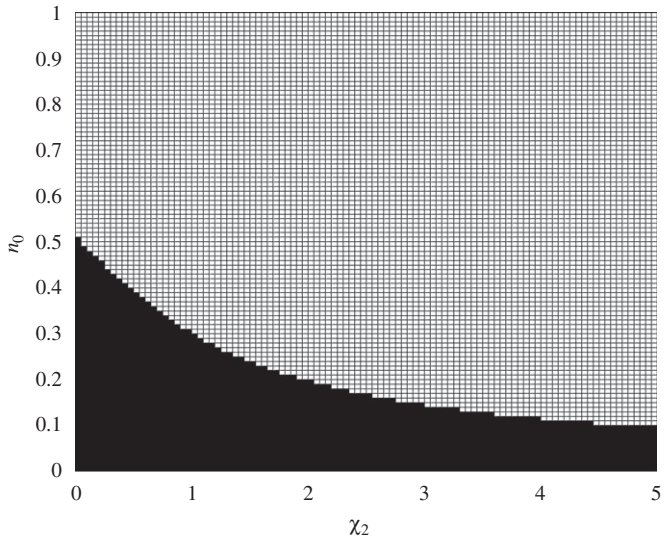


**Fig. 5.** A plot of the stability regions for Hypothesis 1 (see Table 1), with $R=0$. Black (white) denotes regions for which the spatially homogeneous steady state is linearly stable (unstable) to perturbations of all (certain) wavenumbers. Parameter values: $R=0$, $D_n=D_m=0.5$, $\phi=0.5$, $\gamma_2=1$, $m_0=1-n_0$.

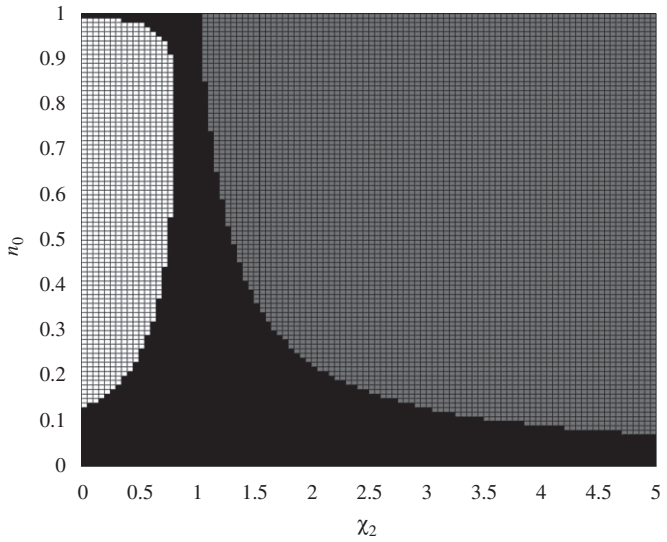


**Fig. 6.** A plot of the stability regions for Hypothesis 1 (see Table 1). In black regions both roots of $\omega$ are real and negative for all $q$, whilst dark grey denotes regions where complex conjugate roots can exist, but have negative real part. Hence in both the spatially homogeneous steady state is linearly stable to perturbations of all wavenumbers. In white regions the roots can be real and of differing sign (so the homogeneous state is linearly unstable to perturbations of certain wavenumbers). Parameter values: $R=100$, $r=0.1$, $D_n=D_m=0.1$, $\phi=0.1$, $\gamma_2=1$, $m_0=1-n_0$.

This curve can be plotted in *e.g.* $(n_0,\chi_2)$ space, and validates the results presented in Fig. 5 (comparison not shown).

We now assume $R>0$, in which case the coefficients in Eq. (3.8) are given by (3.13) and

$$C=(q^2D_m+2qm_0Rr\Psi(qr))\left(q^2D_n+2qn_0Rr\Psi(qr)-\frac{q^2n_0}{q^2+1}\right)-q^2n_0m_0\left(\frac{q\chi_2a^2}{a^2q^2+1}-2Rr\Psi(qr)\right)\left(\frac{q\phi}{q^2+1}-2Rr\Psi(qr)\right). \quad (3.21)$$

As before, a sufficient condition for instability is $C<0$. We note that $B>0$, $C>0$ in the limit as $q\to\infty$, (since $\Psi(qr)\to\pi/2$ as $q\to\infty$ Abramowitz and Stegun, 1970). Hence the model remains linearly stable to perturbations of large wavenumber. However, we observe that the introduction of the repulsion terms can lead to the apparently paradoxical behaviour where increasing the strength of hepatocyte–stellate attraction ($\chi_2$) is stabilising (see Fig. 6). To understand why this can occur, let us assume that $D_n=D_m=0$ (it will subsequently be obvious that our arguments also apply when $0<D_n, D_m\ll 1$), and that the repulsion strength $R$ is sufficiently large that $B(q)>0$ for all $q$. Under these assumptions, we see from Eq. (3.21) that when $\chi_2=0$, the terms quadratic in $R$ cancel, and $C<0$ provided that $\phi<1$. As $\chi_2$ is increased, assuming $\phi$ is sufficiently small, $C$ increases and eventually becomes positive. This corresponds to strong repulsion between all cell types, with weak attraction of stellates to hepatocytes. When hepatocyte–stellate attraction is absent (or very weak), hepatocyte–hepatocyte repulsion is weaker than hepatocyte–stellate repulsion (since the former is overcome to some extent by hepatocyte–hepatocyte attraction) and the hepatocytes will aggregate. As the hepatocyte–stellate attraction increases, the difference in strength between hepatocyte–hepatocyte and hepatocyte–stellate repulsion decreases, until eventually the hepatocytes can no longer be pushed together in this way.

In contrast to the $R=0$ case, we note that it is possible to have $B<0<C$, which represents an alternative sufficient condition for instability. Since $\Psi(\cdot)$ is an odd function of its argument, $C$ is an even function of $q$ (and hence it suffices to consider positive $q$). Further, $\Psi(0)=0$; and, since $\Psi'(x)=(1-\cos(x))/x^2\geq 0$, it follows that $\Psi(x)>0$ for $x>0$ (see Fig. 4). We can then say that, if $B<0$, the second bracket of the first term in (3.21) is negative. Hence, with $B<0$, a necessary condition for $C>0$ is that the second term in (3.21) be negative—*i.e.*

$$\left(\frac{q\chi_2a^2}{a^2q^2+1}-2Rr\Psi(qr)\right)\left(\frac{q\phi}{q^2+1}-2Rr\Psi(qr)\right)<0. \quad (3.22)$$

The two bracketed terms above each represent a balance between hepatocyte–stellate attraction and repulsive effects. Thus, if (3.22) is satisfied, either hepatocyte attraction to stellates is weaker than repulsion and stellates experience a net attraction to hepatocytes or *vice versa*.

For there to be complex conjugate roots, we require $B^2<4C$. A Hopf bifurcation occurs when the real part of two complex conjugate roots of (3.8) changes sign. We observe from (3.13) and (3.21) that we can fulfil the conditions $B,C>0$, $B^2-4C<0$ by judicious choice of $D_n$, $D_m$, $\chi_2$ and $\phi$. In this case (3.8) has complex conjugate roots with negative real part. By reducing $D_n$ or $D_m$, we can decrease $B$ through zero, whilst keeping $C>0$ (through appropriate choice of $\chi_2$, $\phi$). Thus a Hopf bifurcation can occur when $R>0$ (in contrast to the $R=0$ case).

Illustrative plots of the stability regions in $(n_0,\chi_2)$ space are shown in Fig. 7.

We are also interested in how the rate of aggregation is affected by the cell seeding ratio, since promoting swift spheroid formation is important for preventing cell de-differentiation and death. We thus use our analysis to determine how $\max\{\Re(\omega(q))\}$ depends on $n_0$ (fixing $m_0=1-n_0$ so the total cell density remains constant). Fig. 8 reveals that, when hepatocyte–hepatocyte chemotaxis is strong relative to hepatocyte–stellate attraction, the greatest rate of aggregation can be achieved by setting $n_0=1$ (solid line)—*i.e.* seeding hepatocytes alone, without stellates. As the attraction between hepatocytes and stellates becomes stronger, the rate of aggregation is improved by increasing the proportion of stellates. When the hepatocyte–stellate attraction becomes very strong, the ideal seeding ratio comes close to 1:1 (dot-dash line).

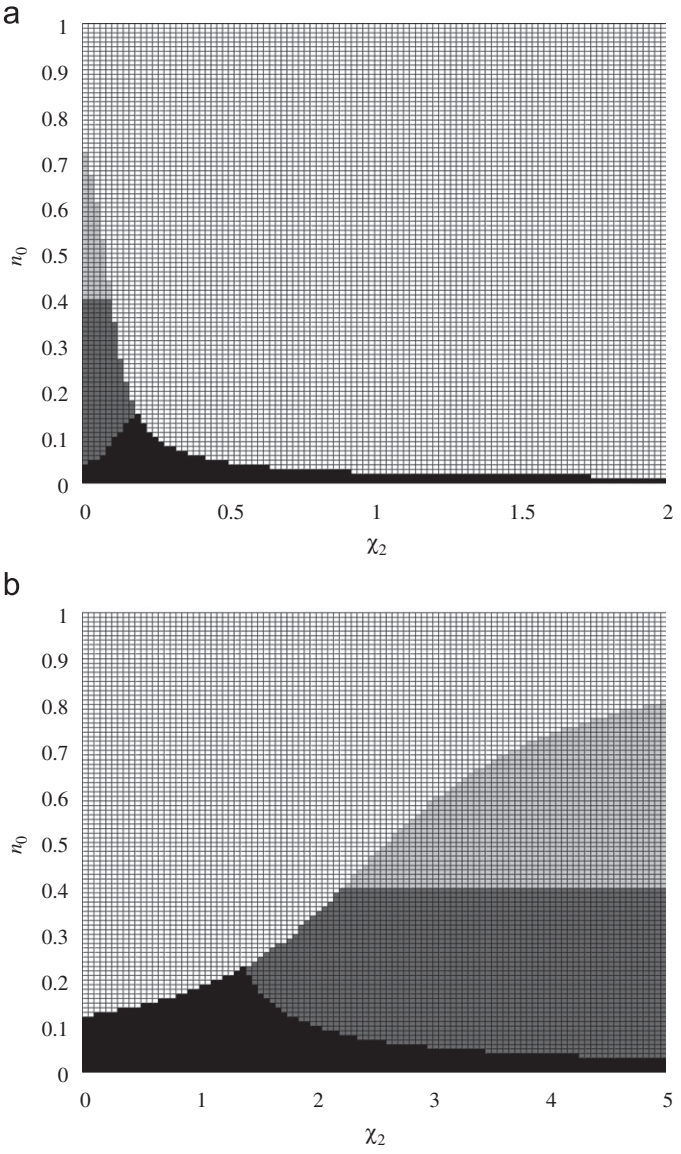


**Fig. 7.** Plots showing how the stability regions change with varying $\phi$ for Hypothesis 1 (see Table 1), with $R>0$. In white regions, the roots of $\omega$ can be real and of differing sign (spatially homogeneous steady state is linearly unstable to perturbations of some wavenumbers). In black regions both roots are real and negative for all $q$ (linearly stable). Dark grey denotes regions where complex conjugate roots can exist, but have negative real part (linearly stable), while light grey denotes regions where complex conjugate roots with positive real part can exist (linearly unstable). Parameter values: (a) $R=20$, $r=0.1$, $D_n=D_m=0.1$, $\phi=2$, $\gamma_2=1$, $m_0=1-n_0$; (b) for (a), with $\phi=0.1$.

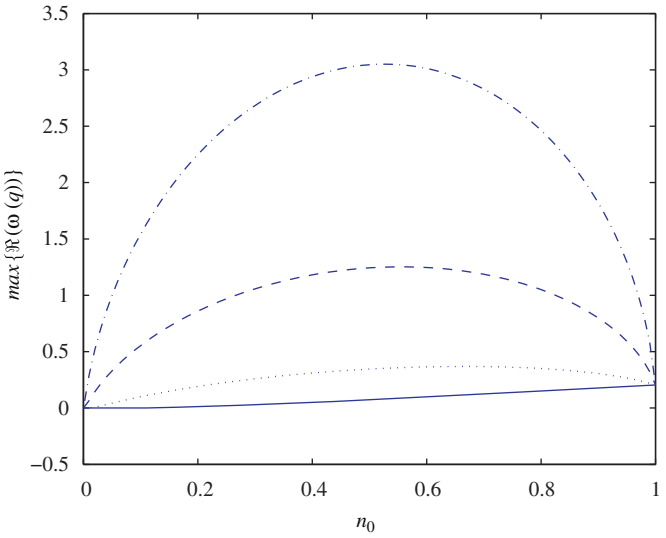


**Fig. 8.** The dependence of maximum growth rate ($\max\{\Re(\omega(q))\}$) on the cell seeding density, $n_0$ for Hypothesis 1 (see Table 1), with $m_0=1-n_0$. Parameter values: $\chi_2=\phi=0.5$ (solid), $\chi_2=\phi=2$ (dot), $\chi_2=\phi=5$ (dash), $\chi_2=\phi=10$ (dot-dash) with $\gamma_2=1$, $R=20$, $r=0.1$ $D_n=D_m=0.1$ in all cases.

### 3.2. Hypothesis 2

We start with the simple case for which $R=0$, and the Fourier transform of the hepatocyte–stellate interaction kernel, $\tilde{K}_{nm}=\tilde{K}_{mn}$, is given by

$$\tilde{K}_{nm}=-2i\mathcal{F}_s(K_{nm})=-2i\int_0^\infty K_{nm}(x)\sin(qx)\,dx$$
$$=2i\frac{A_2}{q}(\cos(qr)-\cos(qa_2)), \tag{3.23}$$

where the dimensionless constants $A_2$ and $a_2$ are as defined in (2.8). The Fourier transform of $K_n$ is given by Eq. (3.11a).

Substituting these forms into the dispersion relation (3.8), we find the coefficient $C$ is given by

$$C=q^4D_m\left(D_n-\frac{n_0}{q^2+1}\right)-4n_0m_0A_2^2(\cos qr-\cos qa_2)^2. \tag{3.24}$$

Applying the same reasoning used in Section 3.1, we deduce that a necessary and sufficient condition for instability is that $C<0$, and hence

$$q^4D_m\left(D_n-\frac{n_0}{q^2+1}\right)<4n_0m_0A_2^2(\cos qr-\cos qa_2)^2. \tag{3.25}$$

As for hypothesis 1, the model is linearly stable to perturbations of large wavenumber ($q\to\infty$), as in this limit inequality (3.25) is violated. For small wavenumbers ($q\ll 1$), inequality (3.25) supplies

$$D_m(D_n-n_0)<n_0m_0A_2^2(a_2^2-r^2)^2. \tag{3.26}$$

Hence, in the biologically realistic case where $a_2\geq r$, instability is more likely to occur if the range of attraction $a_2$ is increased or the range of repulsion $r$ decreased.

For the more general case, $R>0$, we have

$$C=(q^2D_m+2qm_0Rr\Psi(qr))\left(q^2D_n+2qn_0Rr\Psi(qr)-\frac{q^2n_0}{q^2+1}\right)$$
$$-4q^2n_0m_0\left(\frac{A_2}{q}(\cos(qr)-\cos(qa_2))-Rr\Psi(qr)\right)^2. \tag{3.27}$$

For instability, we require either $C<0$ or $B<0<C$. The first condition can once again be interpreted as stating that attractive interactions must be strong enough to overcome diffusion and now also repulsion. The second condition cannot occur, since $B<0$ implies the first term of $C$ is negative, and hence $C<0$. Hence a Hopf bifurcation is not possible in this case, in contrast to Hypothesis 1.

Illustrative stability diagrams in ($n_0$, $A_2$) space are plotted in Fig. 9. As for Hypothesis 1, it is interesting to note the counter-intuitive result from Fig. 9b, that, in certain parameter regimes, increasing the strength of attraction ($A_2$) can be stabilising (*e.g.* for $n_0=0.5$, when $A_2$ is increased from 0 to 1). This can be explained by referring to Eq. (3.27). For simplicity, let us assume that $D_n=D_m=0$ (the arguments also apply when $D_n$, $D_m\ll 1$). If $A_2=0$,

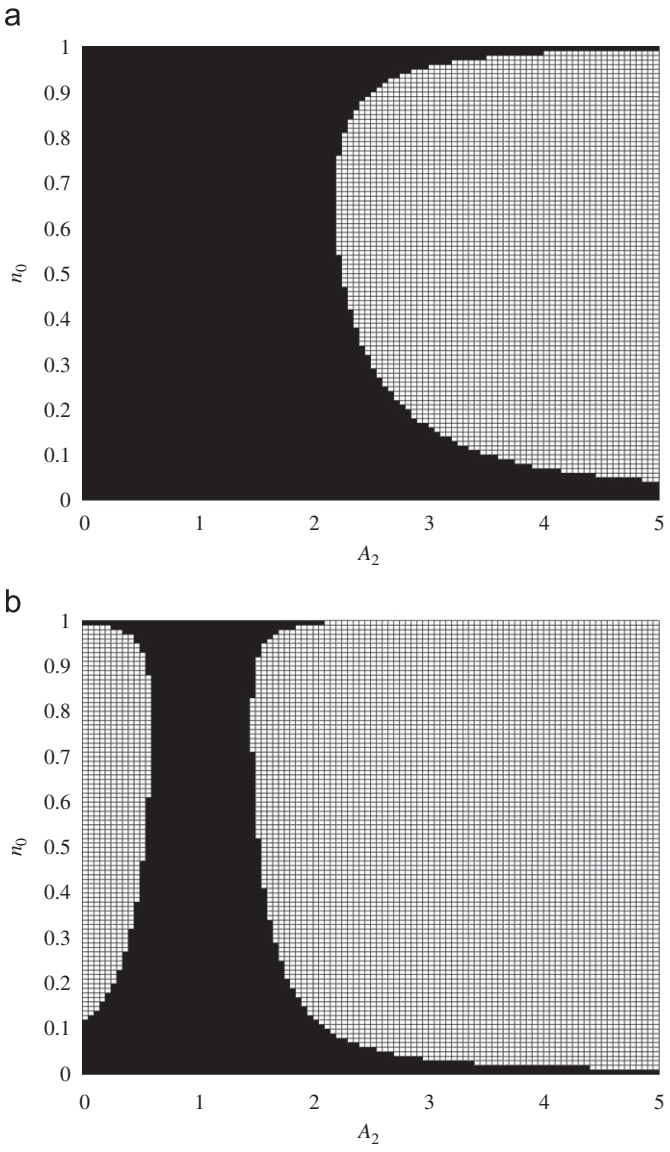


**Fig. 9.** Plots showing how the stability regions change as $D_n=D_m$ varies for Hypothesis 2 (see Table 1). In black (white) the spatially homogeneous steady state is linearly stable (unstable). Parameter values: (a) $R=100$, $r=0.1$, $D_n=D_m=0.4$, $a_2=1$, $m_0=1-n_0$ (b) as for (a), with $D_n=D_m=0.1$.

then (3.27) reduces to give $C=-2q^3n_0m_0Rr\Psi(qr)/(q^2+1)<0$, and hence we conclude the spatially uniform state is unstable. This is because hepatocyte–hepatocyte attraction partially cancels out hepatocyte–hepatocyte repulsion (*i.e.* the term on the second line of Eq. (3.27) increases). Since the hepatocyte–hepatocyte repulsion is the weakest of the interactions, the hepatocytes will tend to cluster together because the hepatocyte–stellate repulsion is stronger than that from each other. As $A_2$ is increased, then hepatocyte–stellate attraction begins to neutralise the effect of hepatocyte–stellate repulsion, and eventually becomes so strong that the difference between hepatocyte–stellate and hepatocyte–hepatocyte repulsion strength effectively disappears. This prevents the hepatocytes from being pushed together and stabilises the spatially uniform steady state. Further increases in $A_2$ will eventually destabilise the spatially uniform state, as hepatocyte–stellate attraction becomes strong enough to overcome the repulsive forces.

When we again consider the effect of the cell seeding ratio on the rate of aggregation, we find that, similar to hypothesis 1, as hepatocyte–stellate attraction becomes stronger relative to hepatocyte–hepatocyte chemotaxis, the value of $n_0$ at which the greatest rate of aggregation reduces towards $n_0=0.5$, which corresponds to a seeding ratio of 1:1 (results not shown).

We conclude this section by noting that the above stability analysis can, potentially, be used to verify our model predictions experimentally. In the context of culturing microvessel endothelial cells, it was noted in Stokes et al. (1990) that increasing the concentration of certain chemicals in the medium can increase the cells' diffusion coefficients. The analysis above suggests that increasing the diffusion coefficients could stabilise an unstable case (though of course, this will depend on the specific parameter values). Chemicals which enhance the random movement of hepatocytes and stellates could be added to the culture medium in the wells, and by thus increasing the cells' diffusion coefficients, prevent aggregation in cases where it would otherwise occur. This would provide validation of our linear stability results. However, care would need to be taken that the culture medium was well mixed, so as to avoid any potential chemotactic effect caused by chemical gradients.

## 4. Numerical simulations

Although the stability analysis allows us to determine the parameter regimes in which aggregation can occur, it does not provide us with information about the distribution of the two cell types within aggregates, nor is it applicable to situations where the cells are not seeded in a spatially uniform manner (*e.g.* where the two types of cells are initially separated by a ring, which is then removed at the start of the experiment or simulation). In order to investigate such questions, we solve the governing Eqs. (2.5) numerically, using the finite element method. Full details of our implementation, and the steps taken to validate the numerical results, are given in the Appendix.

### 4.1. Results

Throughout this section, we set $\varepsilon=0.1$ (giving a spatial domain $-10\le x\le 10$) rather than the value of $10^{-2}$ quoted in Section 2.4. This is to reduce the computational expense of the simulations. Given the boundary conditions stated in Section 2.1, the solutions are periodic, and so this domain truncation should not affect the observed behaviour. We begin by setting the initial conditions to be $n(x,0)=m(x,0)=0.5+0.05\cos(\pi x/10)$, so the cells are seeded in a 1:1 ratio. We observe that, under both hypotheses, three qualitatively different types of behaviour can occur, depending upon the parameter values. We term these: segregation, partial segregation, and intermixing. An illustration of segregation under Hypothesis 1 is shown in Fig. 10. The defining feature is that the hepatocytes, $n$ (Fig. 10(a)), form an aggregate, from the centre of which the stellates (Fig. 10(b)) are excluded ($m\approx 0$ close to $x=0$). In this particular case, hepatocytes are equally strongly attracted to stellates and other hepatocytes, but stellates are only weakly attracted to hepatocytes, and the overcrowding effect is quite strong. As aggregation takes place, the stellate attraction to the hepatocytes is not strong enough to overcome repulsive effects due to overcrowding. As a result, the stellates get 'pushed out' to the edge of the aggregate.

At the opposite extreme an example of intermixing behaviour, obtained under Hypothesis 1, is presented in Fig. 11. Here aggregates form in which the maximum density for both cell types occurs at the same point (though the ratio of the densities is not necessarily 1:1). This behaviour occurs when the hepatocyte–stellate and stellate-hepatocyte attractions are stronger than hepatocyte–hepatocyte attraction and repulsion.

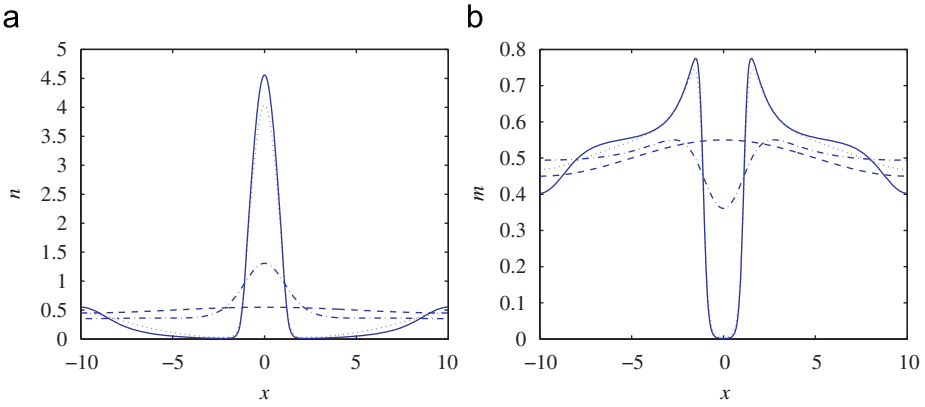


**Fig. 10.** Numerical solution for cell densities $n$ (a) and $m$ (b) under Hypothesis 1 (see Table 1). Times shown: $t=0$ (dash), $t=50$ (dot-dash), $t=100$ (dot) and $t=150$ (solid). Parameter values: $\chi_2=1$, $\phi=0.1$, $\gamma_2=1$, $D_n=D_m=0.1$, $R=20$, $r=0.1$.

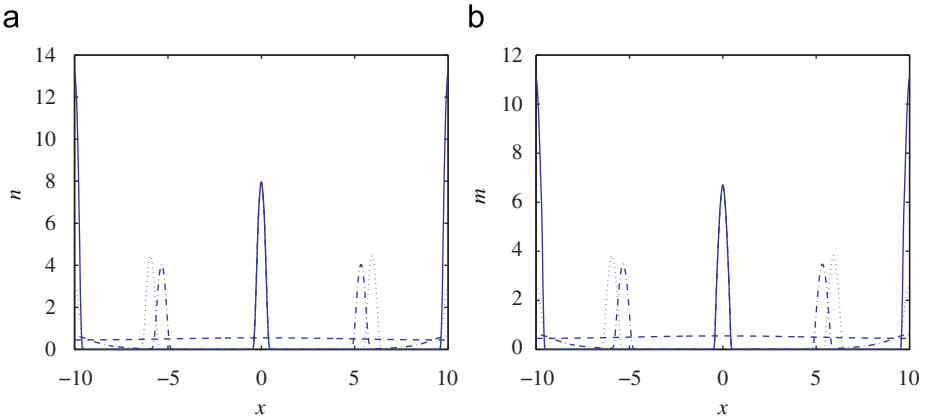


**Fig. 11.** Numerical solution for cell densities $n$ (a) and $m$ (b) under Hypothesis 1 (see Table 1). Times shown: $t=0$ (dash), $t=50$ (dot-dash), $t=100$ (dot) and $t=150$ (solid). Parameter values: $\chi_2=5$, $\phi=5$, $\gamma_2=1$, $D_n=D_m=0.1$, $R=20$, $r=0.1$.

The third type of behaviour, which we term partial segregation, is illustrated in Fig. 12, again under Hypothesis 1. Here aggregates form in which the stellate density is lower in the centre (*i.e.* the point of maximum hepatocyte density) than at the edge, but stellates are present throughout the aggregate.

The preceding results do not enable us to discriminate between the two hypotheses. However, if the two cell types are initially seeded in separate 'clumps' it is possible, for certain parameter values, to observe behaviours which distinguish the two hypotheses. (Experimentally, this pattern could be achieved by seeding the cells within rings, which are subsequently removed, as in Krause et al., 2009.) We consider the initial conditions: $n(x,0)=0.05+0.5\exp(-(x-4)^2)+0.5\exp(-(x+4)^2)$, $m(x,0)=0.05+0.5\exp(-x^2)$, corresponding to a clump of stellate cells seeded in the centre of the domain, with a clump of hepatocytes on either side. If cell–cell attractions are too weak, then, under both hypotheses, the clumps simply spread out to give a uniform density throughout the domain (data not shown). However, under hypothesis 1, if cell–cell attraction is strong enough, the two clumps of hepatocytes merge, forming an aggregate at the centre of the domain. The stellates either aggregate in the same position (this behaviour is illustrated in Fig. 13, where the same parameter values are used as in Fig. 12), or are pushed to the edge of the aggregate as in Fig. 10 (results not shown) depending upon the parameter values. By contrast, under hypothesis 2, the two hepatocyte clumps can move to form three aggregates (centred at the positions of the initial clumps). These three aggregates then merge to form one larger aggregate in the centre of the well, as illustrated in Fig. 14.

## 5. Discussion

In this paper, we have derived a new, non-local model for the interactions between hepatocytes and stellate cells. Two hypotheses were investigated: in the first, stellates and hepatocytes are attracted to each other by chemical signals; in the second, the attraction is assumed to be due to the stellates putting out processes, which make physical contact with the hepatocytes. Under both hypotheses, hepatocytes are attracted to other hepatocytes by a chemical signal, and the effects of overcrowding are incorporated through the non-local repulsion terms.

For both hypotheses, we found that the final distribution of the cells within the aggregates depends upon the relative strengths of attraction and repulsion between the cell types. When hepatocyte–hepatocyte attraction dominates, aggregates have a core consisting of hepatocytes, and repulsion relegates the stellates to the edges of the cluster. Conversely, when hepatocyte–stellate attraction dominates, the two cell types intermix within the aggregates. Intermediate between these two behaviours, 'partial segregation' can occur when hepatocyte–stellate interactions are strong enough to permit the co-existence of both cell types in the aggregate, but repulsion is sufficiently strong to reduce the density of one cell type in the core. We note that in earlier models of cell sorting by chemotaxis (Painter and Sherratt, 2003; Painter, 2009), segregation and intermixing were observed, but not partial segregation. Although Painter and Sherratt (2003) used a similar Keller–Segel type framework, they incorporated overcrowding by making the diffusion and chemotaxis coefficients vanish at a critical cell density, rather than through a non-local term, as here.

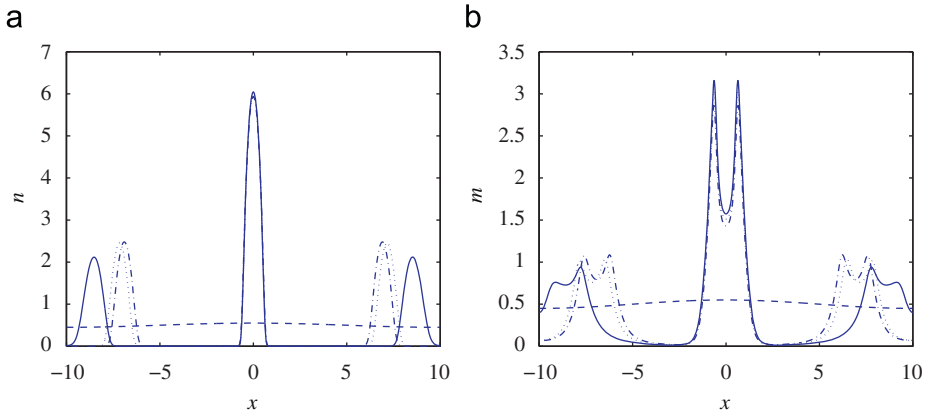


**Fig. 12.** Numerical solution for cell densities $n$ (a) and $m$ (b) under Hypothesis 1 (see Table 1). Times shown: $t=0$ (dash), $t=50$ (dot-dash), $t=100$ (dot) and $t=150$ (solid). Parameter values: $\chi_2=5$, $\phi=1$, $\gamma_2=1$, $D_n=D_m=0.1$, $R=20$, $r=0.1$.

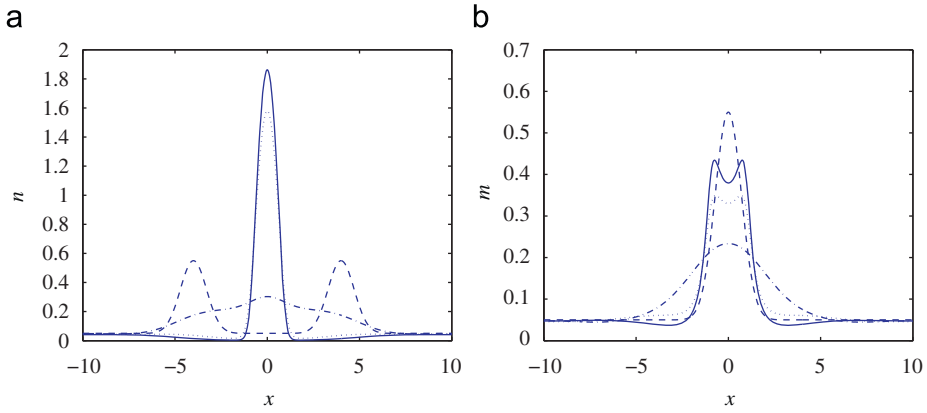


**Fig. 13.** Numerical solution for cell densities $n$ (a) and $m$ (b) under Hypothesis 1 (see Table 1). Times shown: $t=0$ (dash), $t=10$ (dot-dash), $t=30$ (dot) and $t=50$ (solid). Parameter values: $\chi_2=5$, $\phi=1$, $\gamma_2=1$, $D_n=D_m=0.1$, $R=20$, $r=0.1$.

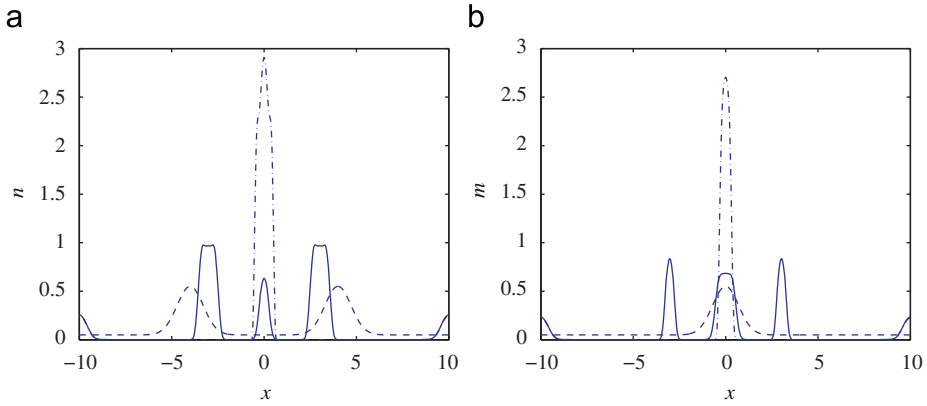


**Fig. 14.** Numerical solution for cell densities $n$ (a) and $m$ (b) under Hypothesis 2 (see Table 1). Times shown: $t=0$ (dash), $t=300$ (solid) and $t=400$ (dot-dash). Parameter values: $A_2=5$, $a_2=1$, $D_n=D_m=0.1$, $R=100$, $r=0.1$.

Our results echo those of the Steinberg hypothesis (or differential adhesion hypothesis (DAH)), where the distribution of cells in aggregates depends upon the relative strengths of the adhesions formed between cells of each type (Steinberg, 1963). Steinberg postulated the existence of a 'free energy' function and proposed that cells can reduce their free energy by forming adhesions. The arrangement of the cells in an aggregate then corresponds to a minimum of the free energy of the system. His predictions have been validated experimentally, using detailed measurements of cadherin (a cell adhesion molecule) (Foty and Steinberg, 2005). A continuum model of this phenomenon has recently been proposed by Armstrong et al. (2006). They applied a non-local framework similar to that used in this paper, with the non-local terms modelling adhesion forces. However, we also note that both our model (under hypothesis 1) and the models of Painter and Sherratt (2003), Painter (2009) display similar cell sorting based on the cells having different affinities for the chemoattractants. This suggests that it may be of interest to explore (experimentally, and through modelling) how differential adhesion and chemotaxis might interact to produce different

tissue architectures. Can the two phenomena combine to produce new patterns and behaviours?

One of the main aims of this paper was to compare the predictions of our models with experimental results, particularly in relation to the distribution of hepatocytes and stellates within spheroids (Thomas et al., 2006). Fig. 15 shows the location of the stellate cells (stained green) within five different aggregates. Comparison of these images with our theoretical results leads us to reject the possibility that hepatocyte–hepatocyte attraction is the strongest effect, since we do not observe a clear segregation of the two cell types into a hepatocyte-only core surrounded by stellates. Instead, stellates can be found both in the centre and at the edges of the aggregates. However, it is not clear whether the images in Fig. 15 represent intermixing or partial segregation. Part of the difficulty is the fact that our model is continuous, whilst, in practice, cells are discrete; consequently we could not expect an even intermixing of the two types. This question could be resolved by measuring the variation in densities of the two cell types across the spheroid radius in a large number of spheroids.

Intuitively, we might expect attraction between the two cell types to dominate hepatocyte–hepatocyte attraction, as there would otherwise be little reason to add the stellates (replacing them with more hepatocytes would have a greater effect). Our results are consistent with this idea; indeed, they suggest that the optimal ratio of the seeding densities of the two cell types to promote swift aggregation is close to 1:1 (see Fig. 8). Experimental research carried out by Riccalton-Banks (2002) found that a 2:1 ratio of hepatocytes to stellates resulted in the formation of greater numbers of aggregates than did ratios of 5:1, 10:1, or hepatocyte-only cultures, which is consistent with our results. However, we remark that in the liver *in vivo* the ratio is approximately 20:1, and thus if considerations other than promoting swift aggregation are taken into account (*e.g.* optimising the functionality of the spheroids produced) there may be good reasons to opt for a higher ratio. At present, experimental evidence on how the numbers of stellates within a spheroid affects its functionality or viability is limited. Riccalton-Banks (2002) compared the functionality of hepatocyte-only and hepatocyte–stellate (2:1 ratio) spheroids and found that the co-cultured spheroids remained functional (in terms of albumin secretion and cytochrome P-450 enzyme activity) for nearly two months, compared to just over one month for the hepatocyte-only spheroids. Krause et al. (2009) reported improved functionality (measured by phosphoenolpyruvate carboxykinase (PCK) activity) in short-term (48 h) 2D co-cultures. The improvement was greatest when the culture arrangements allowed for physical contact between the two cell types, and a hepatocyte:stellate ratio of 1:4 was used. Although differences in culture protocols (*e.g.* 3D versus 2D, different measures of functionality) make it difficult to compare these studies, their evidence suggests that the presence of the stellate cells has a positive impact on the functionality of the engineered tissue, and we thus recommend that the effects on aggregation of culturing hepatocytes and stellates at higher ratios be tested experimentally.

Based on the currently available data, we are unable to distinguish between the two hypotheses, as the cells are initially intermixed and seeded in a spatially uniform way. However, our model results suggest how initial conditions in which the two cell types are seeded in distinct clumps might be used to discriminate between the two hypotheses, since they can produce different behaviours.

The results we have obtained here are only qualitative, and a great deal of further experimental data is required before quantitative model predictions can be obtained. In particular, the correct functional forms for the kernel functions describing the interactions between cells need to be determined. This could be achieved by measuring the forces acting between two cells, and utilising the connection between the individual cell- and

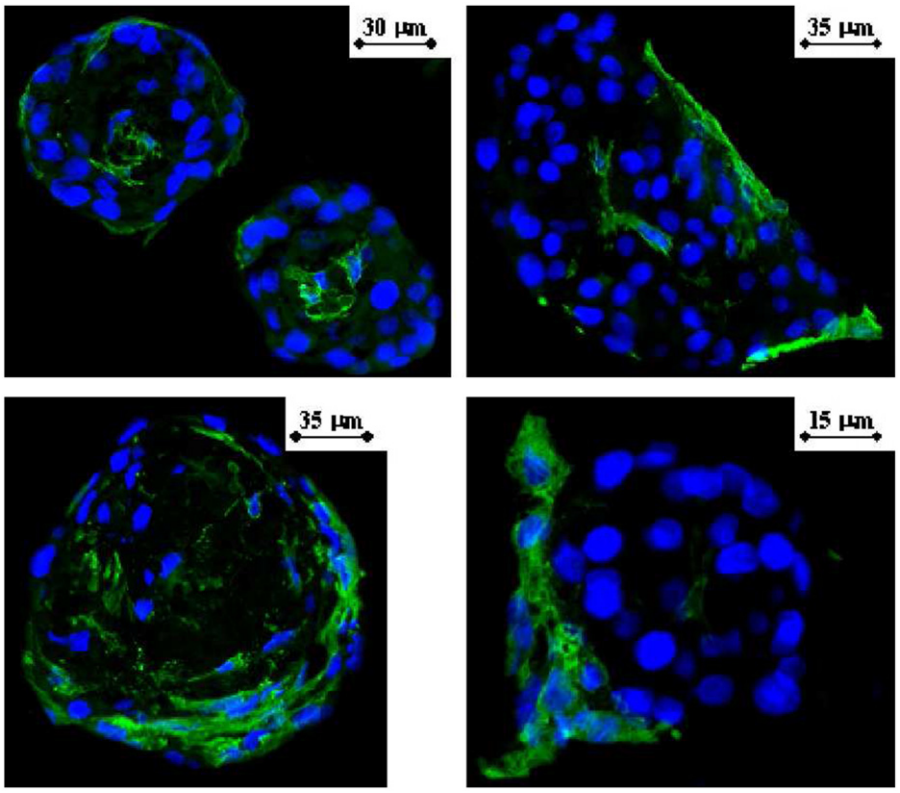


**Fig. 15.** Sections through hepatocyte–stellate cell spheroids (reproduced from Thomas et al., 2006). Stellate cells appear green. (For interpretation of the references to color in this figure legend, the reader is referred to the web version of this article.)

continuum-level descriptions discussed in Section 1. Another interesting approach would be to compare the results of our continuum model with those of an individual-based model similar to that described in Mogilner et al. (2003). The latter might provide better agreement with the experimental results. The most obvious improvement to the model would be to extend it to more physically realistic two- and three-dimensional geometries and determine the types of patterns which may arise in such cases. We might also relax the assumption that the strength of cell–cell repulsion (and in hypothesis 2, cell–cell attraction) is the same for the two cell types. In fact, this may not be so due to one cell type being physically smaller, or more strongly adhered to the substrate. The effects of cell proliferation and death, and nutrient availability, could also be considered.

From a mathematical viewpoint, a number of questions remain to be investigated. For example, integro-PDE models can display interesting behaviour on an exponentially long timescale (see *e.g.* Mogilner and Edelstein-Keshet, 1999). In our numerical simulations, we simulate until the solution changes extremely slowly; we have not yet considered how it might evolve on a much longer timescale. We justify this by noting that such long timescales would be beyond the biologically relevant regime of our model, since we would expect cell proliferation and death to become important. Similarly, we have not proven that steady state solutions of the model equations exist. Since interest in non-local models, with a variety of biological applications, is increasing—see *e.g.* Armstrong et al. (2006), Gerisch and Chaplain (2008), and Szymanska et al. (2009)—placing these models on a more secure theoretical footing will be an important avenue for future research. Some work has already been undertaken in this direction: *e.g.* a recent paper Sherratt et al. (2008) has addressed the question of the boundedness of the solution for a similar single cell population integro-PDE model. However, for two cell population models, these questions remain open.

## Acknowledgements

The work described in this paper was initiated whilst JEFG was visiting LEK at the University of British Columbia, supported by a Special Award from the Royal Commission for the Exhibition of 1851, and parts of it were presented in JEFG's Ph.D. Thesis (Green, 2006), which was funded by a BBSRC studentship (no. 02B1E08683). HMB, SLW and KMS received support from EPSRC Advanced Research Fellowships. The authors thank Dr R.J. Thomas (Tissue Engineering Group, University of Nottingham) for helpful discussions.

## Appendix A. Numerical methods

Given a timestep $\Delta_t$ we compute a numerical solution of the governing equations (2.5) at times $t_j = j\Delta_t, j = 1,2,3,\ldots$. We use the following notation for the solution for $n$, $m$, $c_1$, $c_2$ at time $t_j$:

$$n^{(j)}(x) = n(x,t_j), \quad m^{(j)}(x) = m(x,t_j), \quad c_1^{(j)}(x) = c_1(x,t_j), \quad c_2^{(j)}(x) = c_2(x,t_j).$$

On timestep $j$ we discretise equations (2.5) in time as follows:

$$\frac{n^{(j)} - n^{(j-1)}}{\Delta_t} + \frac{\partial}{\partial x}\left(n^{(j)}\frac{\partial c_1^{(j)}}{\partial x}\right) + \chi_2\frac{\partial}{\partial x}\left(n^{(j)}\frac{\partial c_2^{(j)}}{\partial x}\right) + \frac{\partial}{\partial x}[n^{(j)}(K_n * n^{(j-1)}) + n^{(j)}(K_{nm} * m^{(j-1)})] = D_n\frac{\partial^2 n^{(j)}}{\partial x^2}, \tag{A.1a}$$

$$\frac{m^{(j)} - m^{(j-1)}}{\Delta_t} + \phi\frac{\partial}{\partial x}\left(m^{(j)}\frac{\partial c_1^{(j)}}{\partial x}\right) + \frac{\partial}{\partial x}[m^{(j)}(K_m * m^{(j-1)}) + m^{(j)}(K_{mn} * n^{(j-1)})] = D_m\frac{\partial^2 m^{(j)}}{\partial x^2}, \tag{A.1b}$$

$$\frac{\partial^2 c_1^{(j)}}{\partial x^2} + n^{(j)} - c_1^{(j)} = 0, \tag{A.1c}$$

$$\frac{\partial^2 c_2^{(j)}}{\partial x^2} + m^{(j)} - \gamma_2 c_2^{(j)} = 0, \tag{A.1d}$$

*i.e.* the time derivatives are approximated using a finite difference over the interval $t_{j-1} < t < t_j$, and all other terms are approximated at time $t_j$ with the exception of the kernels. We justify this choice of time discretisation later in this section.

The discretised system above is solved using the continuous Galerkin finite element method: see, for example, (Eriksson et al., 1996). We set $\varepsilon = 0.1$, giving a spatial domain $-10 \le x \le 10$. In all simulations 1000 equally sized elements were used to cover this domain, and linear basis functions were used for each dependent variable on each element. A timestep of 0.001 was used. The resulting system of nonlinear equations was solved using Newton's method.

We evaluate as many terms as possible at time $t_j$ to aid numerical stability. However, the kernels are evaluated at time $t_{j-1}$—where the solution is known—to preserve sparsity of the Jacobian matrix computed using Newton's method. Evaluating these quantities at different times introduces a discretisation error of $\mathcal{O}(\Delta_t)$, which is the same order as that already introduced by discretising the time derivatives.

The code was verified in two different ways. First, we compared the growth rates of the numerical solutions for short times (up to $t = 0.1$) with those predicted by the linear stability analysis for a number of test cases. Excellent agreement was found in each case (data not shown). In addition, for all simulations shown in this paper, we repeated the simulations using twice as many elements and half the timestep specified above, and verified that the plots shown were indistinguishable.

## References

Abramowitz, M., Stegun, I.A. (Eds.), 1970. Handbook of Mathematical Functions, ninth ed. Dover.
Abu-Absi, S.F., Friend, J.R., Hansen, L.K., Hu, W.S., 2002. Structural polarity and functional bile canaliculi in rat hepatocyte spheroids. Exp. Cell Res. 274, 56–67.
Armstrong, N.J., Painter, K.J., Sherratt, J.A., 2006. A continuum approach to modelling cell–cell adhesion. J. Theor. Biol. 243 (1), 98–113.
Bhandari, R.N., Riccalton, L.A., Lewis, A.L., Fry, J.R., Hammond, A.H., Tendler, S.J.B., Shakesheff, K.M., 1997. Liver tissue engineering: a role for co-culture systems in modifying hepatocyte function and viability. Tissue Eng. 7, 345–357.
Billingham, J., 2004. Dynamics of a strongly non-local reaction–diffusion population model. Nonlinearity 17, 313–346.
Bodnar, M., Velazquez, J.J.L., 2005. Derivation of macroscopic equations for individual cell-based models: a formal approach. Math. Meth. Appl. Sci. 28, 1757–1779.
Eriksson, K., Estep, D., Hansbo, P., Johnson, C., 1996. Computational Differential Equations, second ed. Cambridge University Press.
Foty, R.A., Steinberg, M.S., 2005. The differential adhesion hypothesis: a direct evaluation. Dev. Biol. 278, 255–263.
Gentilini, A., Marra, F., Gentilini, P., Pinzani, M., 2000. Phosphatidylinositol-3 kinase and extracellular signal-regulated kinase mediate the chemotactic and mitogenic effects of insulin-like growth factor-1 in human hepatic stellate cells. J. Hepatol. 32, 227–234.
Gerisch, A., Chaplain, M.A.J., 2008. Mathematical modelling of cancer cell invasion of tissue: local and non-local models and the effect of adhesion. J. Theor. Biol. 250 (4), 684–704.
Gourley, S.A., Chaplain, M.A.J., Davidson, F.A., 2001. Spatio-temporal pattern formation in a non-local reaction–diffusion equation. Dyn. Sys. 16 (2), 173–192.
Green, J.E.F., 2006. Mathematical modelling of cell aggregation in liver tissue engineering. Ph.D. Thesis, University of Nottingham, UK.
Green, J.E.F., Waters, S.L., Shakesheff, K.M., Byrne, H.M., 2009. A mathematical model of liver cell aggregation *in vitro*. Bull. Math. Biol. 71 (4), 906–930.

Krause, P., Saghatolislam, F., Koenig, S., Unthan-Fechner, K., Probst, I., 2009. Maintaining hepatocyte differentiation *in vitro* through co-culture with hepatic stellate cells. In Vitro Cell. Dev. Biol. Anim. 45, 205–212.

Lee, C.T., Hoopes, M.F., Diehl, J., Gilliland, W., Huxel, G., Leaver, E.V., McCann, K., Umbanhowar, J., Mogilner, A., 2001. Non-local concepts and models in biology. J. Theor. Biol. 210, 201–219.

Luca, M., Chavez-Ross, A., Edelstein-Keshet, L., Mogilner, A., 2003. Chemotactic signalling, microglia and Alzheimer's disease senile plaques: is there a connection? Bull. Math. Biol. 65 693–730.

Mitaka, T., 1998. The current status of primary hepatocyte culture. Int. J. Exp. Pathol. 79, 393–409.

Mogilner, A., 1995. Modelling spatio-angular patterns in cell biology. Ph.D. Thesis, University of British Columbia, Vancouver, Canada.

Mogilner, A., Edelstein-Keshet, L., 1999. A non-local model for a swarm. J. Math. Biol. 38, 534–570.

Mogilner, A., Edelstein-Keshet, L., Bent, L., Spiros, A., 2003. Mutual interactions, potentials and individual distance in a social aggregation. J. Math. Biol. 47, 353–389.

Painter, K.J., 2009. Continuous models for cell migration in tissues and applications to cell sorting via differential chemotaxis. Bull. Math. Biol. 71, 1117–1147.

Painter, K.J., Sherratt, J.A., 2003. Modelling movement of interacting cell populations. J. Theor. Biol. 225, 327–339.

Riccalton-Banks, L., Liew, C., Bhandari, R., Fry, J., Shakesheff, K., 2003. Long-term culture of functional liver tissue: three-dimensional coculture of primary hepatocytes and stellate cells. Tissue Eng. 9 (3), 401–409.

Riccalton-Banks, L.A., 2002. Maintenance of primary rat hepatocytes in vitro using co-culture techniques. Ph.D. Thesis, University of Nottingham.

Richert, L., Binda, D., Hamilton, G., Viollon-Abadie, C., Alexandre, E., Bigot-Lasserre, D., Bars, R., Coassolo, P., LeCluyse, E., 2002. Evaluation of the effect of culture configuration on morphology, survival time, antioxidant status and metabolic capacities of cultured rat hepatocytes. Toxicol. In Vitro 16, 89–99.

Selden, C., Khalil, M., Hodgson, H.J.F., 1999. What keeps hepatocytes on the straight and narrow? Maintaining differentiated liver function. Gut 44, 443–446.

Sherratt, J.A., Gourley, S.A., Armstrong, N.J., Painter, K.J., 2008. Boundedness of solutions of a non-local reaction–diffusion model for adhesion in cell aggregation and cancer invasion. Euro. J. Appl. Math. 20, 123–144.

Skrtic, S., Wallenius, V., Ekberg, S., Brenzel, A., Gressner, A.M., Jansson, J., 1999. Hepatocyte-stimulated expression of hepatocyte growth factor (HGF) in cultured rat hepatic cells. J. Hepatol. 30, 115–124.

Steinberg, M.S., 1963. Reconstruction of tissues by dissociated cells. Science 141 (3579), 401–408.

Stokes, C.L., Rupnick, M.A., Williams, S.K., Lauffenburger, D.A., 1990. Chemotaxis of human microvessel endothelial cells in response to acidic fibroblast growth factor. Lab. Invest. 63 (5), 657–668.

Stolz, D.B., Michalopoulos, G.K., 1997. Synergistic enhancement of EGF, but not HGF, stimulated hepatocyte motility by TGF-β1 *in vitro*. J. Cell. Physiol. 170, 57–68.

Szymanska, Z., Morales-Rodrigo, C., Lachowicz, M., Chaplain, M.A.J., 2009. Mathematical modelling of cancer invasion of tissue: the role and effect of nonlocal interactions. Math. Models Meth. Appl. Sci. 19 (2), 257–281.

Thomas, R.J., Bhandari, R., Barrett, D.A., Bennett, A.J., Fry, J.R., Powe, D., Thomson, B.J., Shakesheff, K.M., 2005. The effect of three-dimensional co-culture of hepatocytes and hepatic stellate cells on key hepatocyte functions *in vitro*. Cells Tissues Organs 181 (2), 67–79.

Thomas, R.J., Bennett, A., Thomson, B., Shakesheff, K.M., 2006. Hepatic stellate cells on poly(DL-lactic acid) surfaces control the formation of 3D hepatocyte co-culture aggregates *in vitro*. Euro. Cell. Mater. 11, 16–26.